ELSEVIER

Ceramics International 32 (2006) 849–856

CERAMICS INTERNATIONAL

www.elsevier.com/locate/ceramint

# Microstructure and properties of (SiC, $TiB_2$)/$B_4C$ composites by reaction hot pressing

Aiju Li [a,*], Yuhua Zhen [b], Qiang Yin [a], Laipeng Ma [a], Yansheng Yin [c]

[a] *Key Laboratory for Liquid Structure and Heredity of Materials, Ministry of Education of China, Engineering Ceramics Key Laboratory of Shandong Province, Shandong University, Jinan 250061, China*
[b] *Department of Materials Engineering, Tsinghua University, Beijing 100084, China*
[c] *Institute of Materials Science and Engineering, Ocean University of China, Qingdao 266003, China*

Received 25 February 2005; received in revised form 18 March 2005; accepted 30 May 2005
Available online 2 September 2005

**Abstract**

($SiC$, $TiB_2$)/$B_4C$ composites were fabricated by reactive hot-pressing $B_4C$, $Si_3N_4$, α-SiC and TiC powders, with ($Al_2O_3 + Y_2O_3$) as sintering additives. According to the thermodynamics principles, the possible reaction equations and the reaction products for the system were determined. By means of XRD, SEM of surface thermally etched and TEM the phase composition was determined. It was shown that the phase composition of sintered body was $B_4C$, α-SiC, BN and $TiB_2$, and the matrix was $B_4C$ and α-SiC. The typical values of hardness, bending strength, fracture toughness and the relative density of the composites can reach HRA 88.6, 554 MPa, 5.6 MPa $m^{1/2}$ and 95.6%, respectively. Furthermore, the microstructures of the composites were analyzed by TEM, SEM and energy spectrum methods. The results show the presence of laminated structure and a clubbed frame dispersion phase and bunchy dispersion phase among the matrix. Some intragranular structures were also found in the $B_4C$ grains. Microstructural analysis indicates that the new formed phase, uniform and fine grains, and the layered and clubbed structure play an important role in improving the properties of the composites. Fractography and crack propagation suggest that crack deflection and crack bridging are the possible toughening mechanisms.
© 2005 Elsevier Ltd and Techna Group S.r.l. All rights reserved.

*Keywords:* B. Composites; D. SiC; $B_4C$; Reactive sintering; $Ti_2B$

Boron carbide ($B_4C$) ceramics have some excellent physical and chemical properties, such as ultrahigh hardness, low density, excellent chemical stability and neutron absorption capability. But it is difficult to obtain a sintered body with high density, due to covalent bond. Even when sintered around melting point, few substance transport can occur, and the relative density of the sintered body usually is under 80%, together with grain abnormal growth and surface melting [1,2]. Hot pressing, hot isostatic pressing (HIP) and activated a sintering with carbonization are used to obtain a sintered body with a density that could be above 90% [3,4]. However, the sintering temperature is usually above 2160 °C. Meanwhile, many research works have been made to improve its low strength and fracture toughness and to reduce the sintering temperature in the recent years. It has been shown that a secondary phase added in the $B_4C$ matrix can serve as reinforcing and toughening phase, which can also reduce the sintering temperature. Deng and Zhou [5] added (W, Ti)C solid solution into $B_4C$ to prepare (W, Ti)C/$B_4C$ composites by hot pressing at 1900 °C, the fracture toughness of which is 3.9 MPa $m^{1/2}$. Yamada and Hirao [6] used $CrB_2$ as secondary phase to reinforce $B_4C$ matrix and prepared a composite, whose bending strength and fracture toughness are 640 MPa and 3.2 MPa $m^{1/2}$ with the sintering temperature of 2050 °C. However, Tang et al. [7] used PCS as precursor to prepare a SiC/$B_4C$ composite by hot pressing (sintering temperature: 1900 °C), obtaining a fracture toughness of 4.99 MPa $m^{1/2}$.

The research works mentioned above either followed the route of adding a secondary phase into $B_4C$ matrix directly or that of using complicated technology and higher sintering

* Corresponding author. Tel.: +86 531 88395881; fax: +86 531 82940969.
*E-mail address:* Liaiju57@sina.com (A.J. Li).

0272-8842/$30.00 © 2005 Elsevier Ltd and Techna Group S.r.l. All rights reserved.
doi:10.1016/j.ceramint.2005.05.022

temperature to prepare the $B_4C$ matrix materials. In the present work, we fabricated (SiC, $TiB_2$)/$B_4C$ composites with improved properties by using a sintering reaction process to produce SiC and $TiB_2$, which were sintered at relatively low temperature. Furthermore, we studied the phase composition, the mechanical properties and the microstructures of the composites.

## 1. Experimental procedure

Commercially available powders were used as starting materials, namely: $B_4C$ (Mudan Jiang No. 2 Grinding Material Company, purity >95%, 3 μm in granularity, including 1 wt.% O, 0.4 wt.% N and other minor metallic impurities); $Si_3N_4$ (Tsinghua University, purity > 92%, 0.8 μm); α-SiC (Tianjin Chemical Reagent Ltd., purity >99%, 2–3 μm); TiC (Shanghai Chemical Reagent Ltd., purity >99%, 5 μm); $Al_2O_3$ (purity > 99%, ~0.38 μm) and $Y_2O_3$ (purity > 99%).

The sample was made from 20 wt.% α-$Si_3N_4$, 10 wt.% ($Al_2O_3$ + $Y_2O_3$), and 60 wt.% $B_4C$. The mixed powders were dry-milled for 15 h at the rate of 380 rpm in planetary high-energy ball miller, followed by passing through 200-mesh sieve. The mixed powders were put into graphite dies, and hot pressing sintered in furnace (High Multi-5000). Table 1 shows the sintering conditions of sample.

The sintered samples were in ∅ 42 mm circular shape, both faces of which were grinded and the hardness was tested using HRA tester (HD-187.5). Then the sample was cut into (i) 3 mm × 4 mm × 30 mm specimens for measuring the bending strength in digital tension and compression (tester LYS-50000) and (ii) 2 mm × 4 mm × 30–40 mm specimens with a notch 2 mm in depth and 0.25 mm in width for measuring the fracture toughness (SENB) in the same tester. The fracture surface and phase distribution were investigated by scanning electron microscope (Hitachi S-2500) and transmission electron microscope (Hitachi S-8000) with an EDS system.

## 2. Phase structure analysis of the composite

### 2.1. Thermodynamic analysis on sintering process

$B_4C$, $Si_3N_4$ and minim SiC, TiC are the main experimental constituents. The reactions in sintering process proceeding under the hot pressing and high-temperature condition, standard Gibbs free energy were adopted as the thermodynamics basic criterion. It is approximately calculated by using thermodynamic data when $T = 298$ K. The calculation equation is $\Delta_r G_m^{\Phi} = \Delta_r H_m^{\Phi} - T\Delta_r S_m^{\Phi}$, and the results are shown in Table 2.

Table 1
The sintering process conditions of samples

| Samples | Sintering temperature (°C) | Pressure (MPa) | Dwell time (min) | Atmosphere |
|---|---|---|---|---|
| BS-1 | 1800 | 30 | 30 | Vacuum |
| BS-2 | 1850 | 30 | 30 | Vacuum |
| BS-3 | 1880 | 30 | 50 | Vacuum |

Table 2
Possible equations and their Gibbs free energy in the system

| No. | Formulas | $\Delta_r G_m^{\Phi}$ (KJ mol$^{-1}$) |
|---|---|---|
| (1) | $Si_3N_4 + 3B_4C = 3SiC + 2N_2\uparrow + 12B$ | $739.7 - 308.95 \times 10^{-3}$ T |
| (2) | $Si_3N_4 + 3B_4C = 3SiC + 4BN + 8B$ | $-269.46 - 57.67 \times 10^{-3}$ T |
| (3) | $B_4C + 2TiC = 2TiB_2 + 3C$ | $-207.93 + 1.39 \times 10^{-3}$ T |
| (4) | $Si_3N_4 = 3Si + 2N_2\uparrow$ | $744.75 - 326.49 \times 10^{-3}$ T |
| (5) | C + Si = SiC | $-73.22 + 7.95 \times 10^{-3}$ T |
| (6) | $2B + N_2 = 2BN$ | $-504.6 + 173.84 \times 10^{-3}$ T |
| (7) | $TiC + 2B = TiB_2 + C$ | $-139.74 + 98.3 \times 10^{-3}$ T |
| (8) | $4B + C = B_4C$ | $-71.55 + 2.09 \times 10^{-3}$ T |
| (9) | $Si_3N_4 + 3C + 4B = 3SiC + 4BN$ | $-484.11 + 44.44 \times 10^{-3}$ T |

In terms of the principle of minimum free enthalpy, the reaction will occur spontaneously when the Gibbs free energy is negative. As shown in Table 2, reactions according to Eqs. (1) and (4) cannot occur when temperature is between 25 and 1880 °C; the exothermal reactions according to Eqs. (2), (3), (5)–(9) can occur spontaneously due to $\Delta_r G_m^{\Phi} < 0$.

Consequently, the final products that could be present in the composite from the reactions mentioned above are $B_4C$, SiC, $TiB_2$ and BN.

### 2.2. Phase distribution analysis

The XRD-spectrum of BS-3 is shown in Fig. 1. It can be seen that the final products are, as expected, $B_4C$, SiC, $TiB_2$ and BN, $B_4C$ and SiC being the major phases. The SEM-image of sample BS-3 after thermally etched at 1200 °C is shown in Fig. 2. The EDS data indicated that the dark-gray equilateral grains are the $B_4C$ matrix (point 2), the bright short rod-like grains are $TiB_2$ (point 1) and the bright equilateral grains are SiC (point 3), in good agreement with XRD results.

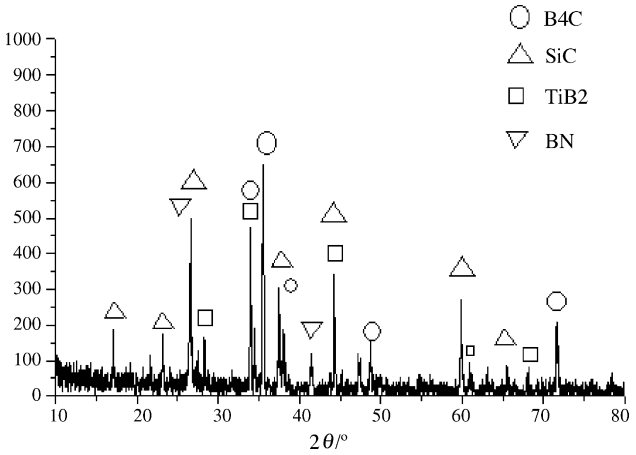


Fig. 1. X-ray diffraction of BS-3.

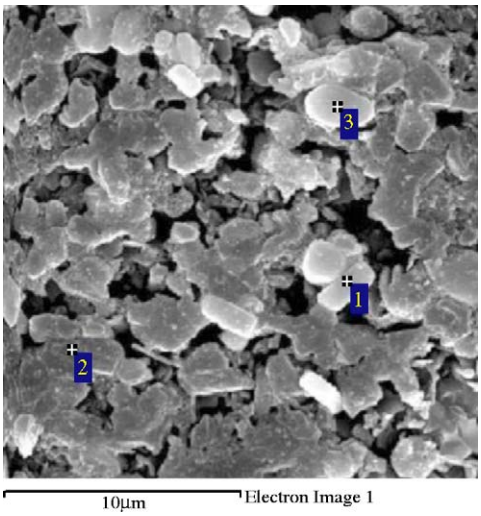


Fig. 2. SEM of surface thermally etched at 1200 °C of BS-3.

A TEM image of sample BS-3 is shown in Fig. 3a. It can be seen that the major phase displays a regular shape. Further analysis shows that point 1 stands for $B_4C$ phase according to the SAD result of point 1 (Fig. 3b) [8].

It can be concluded from the above analysis that the final phases are $B_4C$, SiC, $TiB_2$ and BN, $B_4C$ and SiC being the major phases.

## 3. Properties of the composite

### 3.1. Density and hardness

Fig. 4(a) and (b) show the relative density curve and hardness curve of the samples BS-1–BS-3 at different sintering temperature. It can be seen that the samples have been properly densified when the sintering temperature is higher than 1800 °C. Relative density is typically of the order of 93.5% for this sintering temperature. Meanwhile, the relative density and hardness both increase with increasing temperature. The sample BS-3 displays the highest value with the relative density of 95.6% and hardness of HRA 88.6.

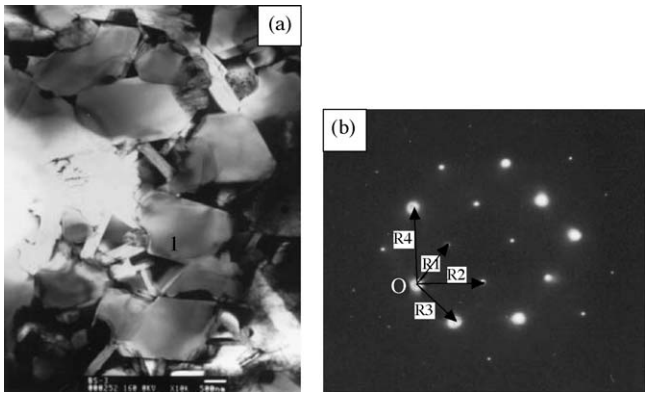


Fig. 3. TEM image of BS3-3 and diffraction spots of point 1.

Since the covalent bond fraction in $B_4C$ is more than 90%, removing of gas phase, grain boundary and volume diffusion and so forth mechanisms all work above 2000 °C. Therefore, it is difficult to obtain dense sintered body. $Al_2O_3$ and $Y_2O_3$ (10 wt.%) as sintering aids are used to decrease sintering temperature and make sample compact. Previous study [9] shows that low-melting compounds such as $Y_3Al_5O_{15}$ (melting point: 1760 °C) and YAlO (melting point: 1850 °C) can form between $Al_2O_3$ and $Y_2O_3$. Under a pressure of 30 MPa and a dwell time of 30–50 min, the sintering materials are in the solid state. Whereas, a liquid phase would form during the sintering process. The liquid phase can fill-up pore space, the gas in the body can diffuse or escape by bubble dropping of the liquid phase, and solid particles can flow greatly due to capillary force, making the particles redistribute and compact.

Another possible explanation of improved density is the contribution of fine particles. It is well known that the more surface energy the particles have, the larger the driving force of sintering is. In general, fine powders possess higher surface energy than large particles. Meanwhile, fine particles can reduce the diffusion length between atoms. Both mechanisms would accelerate the sintering process. SEM image of powders before sintering is shown in Fig. 5. It can be seen that particle size is in sub-micron scale. Size analysis indicates that the powder size $D_{90}$ is 0.38 μm. Sinter driving force and sintering speed rate can be improved greatly using the fine particles, which also tend to sinter compactly.

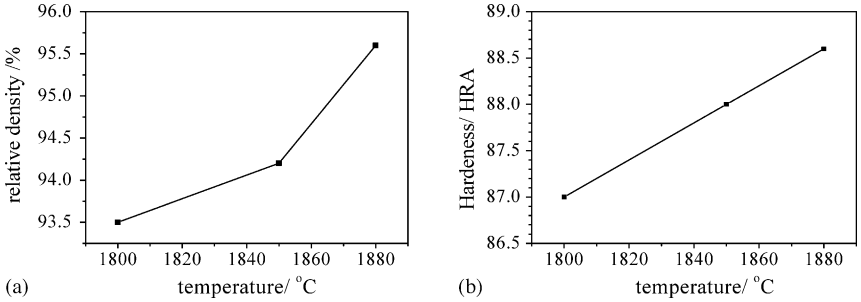


Fig. 4. Relative density curve (a) and hardness curve (b) of the samples sintered at different temperatures.

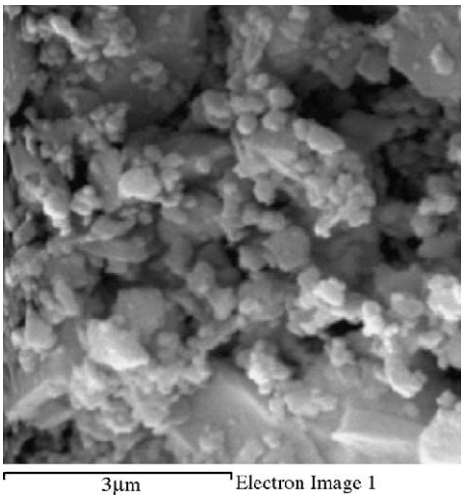


Fig. 5. SEM images of powders.

### 3.2. Bending strength and fracture toughness

Bending strength and fracture toughness of the samples sintered at different temperature are shown in Fig. 6, which are much higher than that of single-phase $B_4C$.

The bending strength and fracture toughness both increase with the increase of sintering temperature, whose maximum value can reach 554 MPa and 5.6 MPa $m^{1/2}$, respectively. Fig. 6(a) shows that the bending strength of the composite reaches its maximum at 1850 °C, but shows slight drop with further increase of the temperature.

## 4. Microstructure of the composite

SEM images of thermally etched surface show that the grain of $B_4C$ is equiaxed, while the grain of $TiB_2$ is rod-like. Besides based on SEM and TEM analyses, it is found that the samples contain laminated structure, rod-like structure, and intragranular structure.

### 4.1. Laminated structure

Fig. 7 shows the SEM images of fracture surfaces of samples BS-1 and BS-3. It can be seen that all the grains of the samples stack with laminated structure, the boundary is not obvious, while pores exist between the boundaries (as indicated by arrows). The oriented arrangement of laminated structure depends on sintering process and crystal structure of materials themselves [10]. New phases α-SiC and BN are obtained in this sintering reaction, which are hexagonal. The crystal plane energy is anisotropic in different crystal directions, making the growth of grains anisotropic. Meanwhile, phases tend to grow preferentially perpendicular to the hot pressing direction due to the fact that the system is under hot pressing condition, and then tend to form the laminated structure.

### 4.2. Shape and distribution of dispersed network phase

Fig. 8 shows the TEM image of the sample BS-3. Some network phases are dispersed among the $B_4C$ matrix, most of which are long rod-like, then form frame structure (as indicated by arrows). Energy spectrum analysis reveals higher content of Si, with little Fe, but it cannot be quantified because the major elements (such as B, C, N) are light elements. Then it is believed that the structure is mainly α-SiC, while Fe may be impurity in the crude materials or dropping-in during ball milling.

Beam-like irregularity structure is also dispersed phase, among the matrix, whose energy spectrum components contain B, C, N, Si, etc. It is believed to be BN based on its pattern and XRD analysis.

### 4.3. Intragranular regular rod-like crystals

Intragranular crystal structure is also observed from the TEM images of the sample BS-3 (as indicated by thick arrows in Fig. 9(a) and (b)). A regular elongated grain in submicron size exists within the $B_4C$ grains. The size of which is different. The ratio of grains is 2–3 according to the scale bar labeled in the figure. Energy spectrum analysis shows that Si is the major element and Fe also exists. The new phase is SiC in terms of the combination of energy spectrum analysis and XRD, whose content is low. Fe is impurity.

Interconnecting dense structure was formed during the process of hot pressing under driving force of sintering, and $B_4C$ matrix grows compact gradually with the new phase

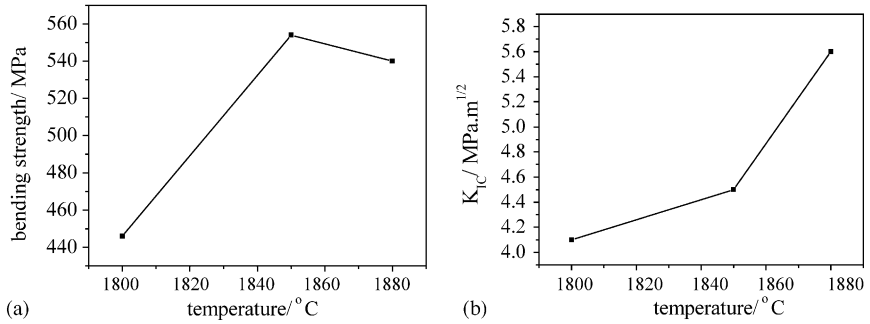


Fig. 6. Bending strength curve (a) and fracture toughness curve (b) of the samples sintered at different temperatures.

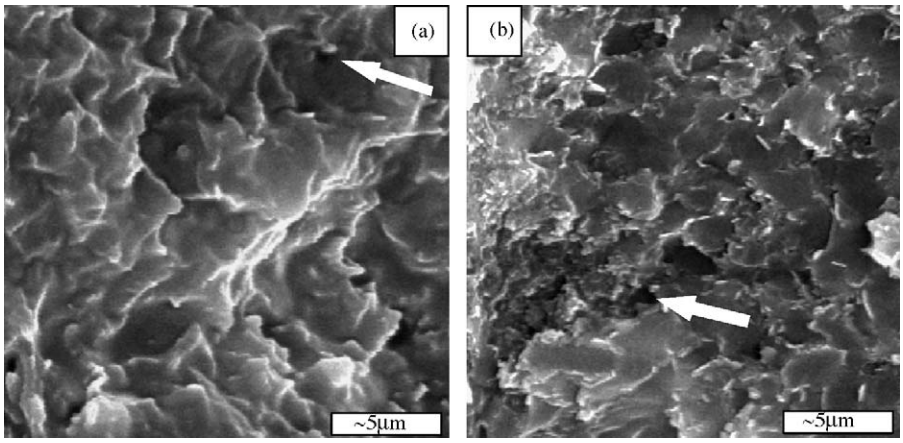


Fig. 7. SEM images of fracture surfaces: (a) BS-3 and (b) BS-1.

α-SiC and so forth diffusing among them. Smaller α-SiC particles on the surface of $B_4C$ particles were trapped into the $B_4C$ grains, and larger grains such as α-SiC, BN and $TiB_2$ resident among the $B_4C$ grains, which form intergranular/intragranular structure.

## 5. Reinforcing and toughening mechanisms

The SEM image of thermally etched surface reveals the fine and uniform (2–3 μm) grains of sintered body. Some frame-like, intragranular structure, bundle-like phase, etc. were formed. Combined with the mechanical properties, the reinforcing and toughening mechanisms of this system are as follows.

### *5.1. Reinforcement by grain refining*

The products can impede the growth of matrix grains and reinforce matrix during the reaction sintering process [11]. Higher temperature is in favor of the formation of new phase trouble-free operation in this experimentation, and generates more SiC, $TiB_2$. It is distributed uniformly in the $B_4C$ matrix, and restricts abnormal growth of $B_4C$ grains, and the new phases have small grain size, then assure higher bending strength and fracture toughness. The increase of TiC and $TiB_2$ also contribute to the improvement of fracture toughness. The more quantity of SiC and $TiB_2$ is produced during the reaction, the more new grain boundary can be formed, the higher grain boundary energy can be reached, and the higher crack propagation resistance can be obtained, the fracture toughness of material is then improved. The sandwich SiC and rod-like $TiB_2$ tend to improve the properties of the composite.

That the bending strength of sample BS-3 sintered at 1880 °C is lower than that of sample BS-2 sintered at 1850 °C in Fig. 6(a) may be attributed to the difference of dwell time. The dwell time of sample BS-3 was 50 min, while the other was 30 min.The longer time and higher sintering temperature of sample BS-3 may lead some abnormal grain growth, as shown in Fig. 10. This large grain is verified to be SiC by energy spectrum analysis (Fig. 10b) together with XRD. That is, some SiC grains grow abnormally due to long dwell time during the sintering reaction. It is usually admitted that relative significant residual stress may occur around the relative large grains,

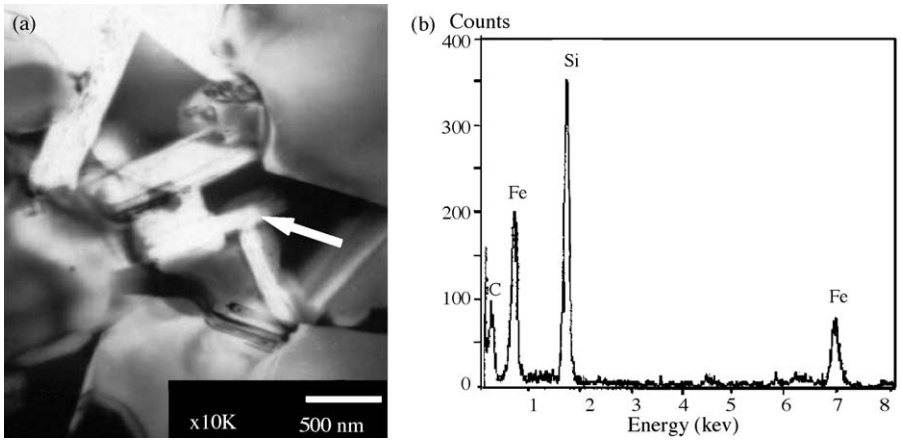


Fig. 8. Long-column structure (a) and EDAX (b) in BS-3.

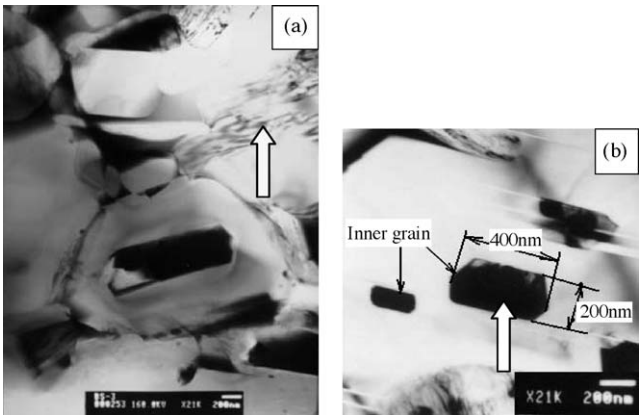


Fig. 9. (a) Fascis structure and (b) intragranular structure in BS3-3.

together with some microcracks and defects, which would deteriorate the mechanical properties of the composites.

### 5.2. Reinforcement by sandwich structure

The anisotropy of growth rate of hexagon α-SiC or BN crystals facilitates the formation of laminated structure or long rod-like crystals and under the condition of hot pressing, major structure tends to be laminated structure, which is distributed uniformly, with low void rate. The fractography can be regarded as compact lamella structure. The special shape can improve toughness of matrix in situ, whose major mechanisms are the adjustment of boundary structure and increase of crack propagated length.

Laminated structure materials have the same fracture mode, as the massive materials and have the maximum strength with strong binding. Cracks can be deflected between lamellas, and the lamella materials would have high-fracture toughness and low-bending strength [12]. To keep high toughness and fracture energy, and have high strength, two ways may be adopted: one is the addition of whiskers and seed crystals into the basic material; the other is the addition of some rod-like crystals into boundary layers to improve bonding strength [13]. Five weight percent α-SiC was added into matrix $B_4C$ to improve preferential growth of new phase α-SiC, and restrain abnormal growth of grains $B_4C$. Some long rod-like α-SiC crystals exist at the boundaries of the composite, which connect each other in frame shape, which can improve both toughness and strength.

### 5.3. Reinforcement by dispersed network phases

As shown in Fig. 8, long rod-like α-SiC with frame structure is dispersed among $B_4C$ matrix in frame shape, which can connect it, fill the gap and strengthen the boundary. The toughening mechanism of long rod-like α-SiC is similar to that of fiber or whisker, which is the crack deflection and bridging.

The beam-like irregular phase BN is loose, with low boundary strength, which can assure that crack tend to deflect when meeting the lamella, increase crack propagation length, and improve the toughness with crack bridging mechanism. However, it also has negative effects on the composite. On the one hand, the porosity would increase due to the difficult sintering of BN. On the other hand, hexagon BN has laminated structure similar to graphite, whose laminated structure is weak bonding molecular structure, then tend to flake off, and decrease the strength of materials.

Rod-like α-SiC with definite slenderness ratio exists in the matrix (as shown in Fig. 9). The intragranular structure tends to induce many sub-interface and microcracks, and make the matrix grains potentially differentiate, then decrease the effect of basic boundary slightly, and induce transgranular fracture. Cracks would not cross the small grains but deflect along the sub-boundary due to small-size, high-strength intragranular crystal, which also can increase crack extension energy, and improve the toughness of matrix. Meanwhile, more sub-boundary can refine and strengthen the matrix [14].

## 6. Fracture mechanisms of the composites

Fig. 11 reveals the crack propagation morphology. The fracture mode is a mixture of transgranular and intergranular fracture. Deflection and bridging could be observed. Such

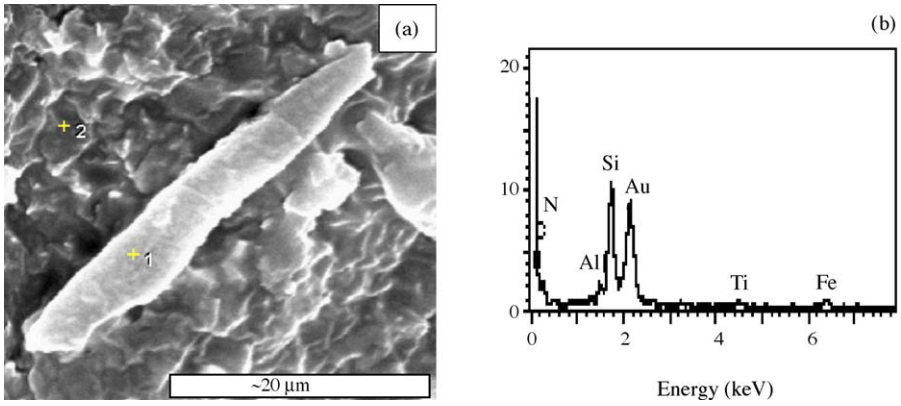


Fig. 10. (a) Abnormal growth of grains and (b) EDAX of element in BS-3.

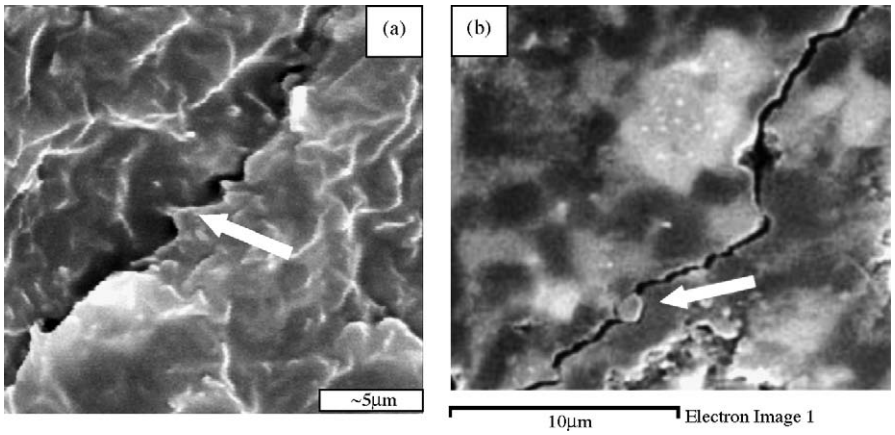


Fig. 11. The crack deflection SEM image of (a) is fracture and (b) is surface in BS-3.

phenomena can be explained by microcracks and stresses that exist in the composite. The $B_4C$ matrix is made of phases with different thermal expansion coefficients (CTE). Taking $TiB_2$ and $B_4C$ for example, the CTE values are $8.1 \times 10^{-6}$ and $4.5 \times 10^{-6}$/°C, respectively. Large internal stress would form when the composite is cooled down from sintering temperature. The internal stress has been measured and reported in literature [15], revealing that the phase formed by in situ reaction brought great compressive stress to matrix. The matrix particles of $B_4C$ (black area in Fig. 11(b)) due to compressive stress were protected, avoiding the transgranular fracture. Meanwhile, $B_4C$ particles tend to induce intergranular fracture for it is well distributed and fine. The transgranular fracture is the major fracture mode in new phases (gray area in Fig. 11(b)), indicating that the binding force of grain boundary was so strong that cracks tend to advance transgranularly, and it can consume more energy. The presence of microcracks can make major cracks deflect and branch, and also make the development of main cracks consume more energy. Consequently, it shows high toughness.

Tensile failure (bridging) by pulling out from matrix can be induced when fracture occurs and the bonding force between the dispersed network phase and basic phase is strengthened, as indicated by arrows in Fig. 11(a), which can improve the toughness of material effectively. The crack propagation may be impeded by fine particles, which could make the cracks propagation deflect during the development of cracks, and this is called the ''shielding/pinning'' effect.

As analyzed above, it is assumed that the fracture mechanisms are the crack deflection and the bridging effect of grains.

## 7. Conclusions

(1) (SiC, $TiB_2$)/$B_4C$ composites were fabricated from $B_4C$ and $Si_3N_4$, a few SiC, TiC with $Al_2O_3 + Y_2O_3$ sintering additive. The maximum value of hardness, bending strength and fracture toughness of the composite is HRA 88.6, 540 MPa and 5.6 MPa $m^{1/2}$, respectively.
(2) According to SEM images of fracture surface, TEM images and mechanical properties, grain refining, laminated structure and dispersed network phases are the major toughening means.
(3) The fracture mechanisms of (SiC, $TiB_2$)/$B_4C$ composite should be crack deflection and crack bridging.

## Acknowledgement

This work was financially supported by key natural science fund of Shandong, China (No.Z2002F02).

## References

[1] K.A. Schwetz, G. Vogt, Process for the production of dense sintered shaped articles of polycrystalline boron carbide by pressureless sintering, U.S. Patent 4195066, 5 March 1980.
[2] S. Prochazka, S.L. Dole, C.I. Hejna, Abnormal grain growth and microcracking in boron carbide, J. Am. Cream. Soc. 68 (9) (1985) 235–236.
[3] D.L. Jiang, Fine Ceramic Materials, China wuzi Publisher, Beijing, 2000, 158–175 (in Chinese).
[4] B.Y. Yin, L.S. Wang, Y.C. Fang, Sintering mechanism of pure and carbon-doped boron carbide, J. Chin. Ceram. Soc. 29 (1) (2001) 68–71 (in Chinese).
[5] J.X. Deng, J. Zhou, Preparation of $B_4C$ (W, Ti) C ceramic composite and study on its mechanical properties, Silic. Bull. 1 (2002) 16–20.
[6] S. Yamada, K. Hirao, Mechanical and electrical properties of $B_4C$-$CrB_2$ ceramics fabricated by liquid phase sintering, Ceram. Int. 29 (3) (2003) 299–304.
[7] J. Tang, S.H. Tan, Z.M. Chen, Toughening $B_4C$ ceramics by $TiB_2$ particles produced in situ $B_4C$, Powder Metall. Technol. 14 (3) (1996) 168–174.
[8] Y.H. Zhen, Study on B4C lighting composite fabricated by reaction hot pressing, Master Dissertation, Shandong University, 2004, pp. 45–61 (in Chinese).
[9] B. Dmitri, R.K. Surya, Microstructural evolution during transient plastic phase processing of titanium carbide-titanium boride composites, J. Am. Ceram. Soc. 79 (7) (1996) 1945–1952.

[10] R. Robert, K.Y. Donaldson, D.P.H. Hasselman, Thermal conductivity of boron carbide-boron nitride composites, J. Am. Ceram. Soc. 75 (10) (1992) 2887–2890.

[11] K.F. Cai, C.W. Nan, The influence of $W_2B_5$ addition on microstructure and thermoelectric properties of $B_4C$ ceramic, Ceram. Int. 26 (2000) 523–527.

[12] S.Y. Cai, J.L. Li, Z.P. Xie, Y. Huang, Influence of interfacial bonding of $Si_3N_4$ laminated composites on the mechanical properties, Acta Materiae Compositae Sinica 16 (2) (1999) 110–115 (in Chinese).

[13] Q.F. Zan, Y. Huang, C.A. Wang, S.Q. Li, C.W. Li, Effect of the rod-like β-$Si_3N_4$ grain and SiC whisker in the $Si_3N_4$/BN multilayer material, Mater. Eng. 5 (2001) 22–26 (in Chinese).

[14] S. Ding, G.W. Wen, T.Q. Lei, Y. Zhou, Microstructures and properties of polycarbosilane transferred nano SiC reinforced B4C matrix composites, J. Inorg. Mater. 17 (5) (2002) 1013–1018 (in Chinese).

[15] S. Ding, G.W. Wen, T.Q. Lei, Y. Zhou, Preparation of nano-micro particles reinforced B4C matrix composites by in-situ reaction, Mater. Eng. 5 (2002) 14–21 (in Chinese).